

# *BeppoSAX* observations of 1-Jy BL Lacertae objects - II

Paolo Padovani<sup>1,2\*</sup>, Luigi Costamante<sup>3,4</sup>, Paolo Giommi<sup>5</sup>, Gabriele Ghisellini<sup>6</sup>,  
Annalisa Celotti<sup>7</sup>, Anna Wolter<sup>8</sup>

<sup>1</sup> *Space Telescope Science Institute, 3700 San Martin Drive, Baltimore MD. 21218, USA*

<sup>2</sup> *Affiliated with the Space Telescope Division of the European Space Agency, ESTEC, Noordwijk, The Netherlands*

<sup>3</sup> *Università degli Studi di Milano, Via Celoria 16, I-20133 Milano, Italy*

<sup>4</sup> *Max-Planck Institute für Kernphysik, Postfach 10 39 80, D-69029 Heidelberg (current address)*

<sup>5</sup> *ASI Science Data Center, ASDC, c/o ESRIN, Via G. Galilei, I-00044 Frascati, Italy*

<sup>6</sup> *Osservatorio Astronomico di Brera, Via Bianchi 46, I-23807 Merate, Italy*

<sup>7</sup> *SISSA, via Beirut 2-4, I-34014 Trieste, Italy*

<sup>8</sup> *Osservatorio Astronomico di Brera, Via Brera 28, I-20121 Milano, Italy*

Accepted , Received

## ABSTRACT

We present new *BeppoSAX* LECS and MECS observations, covering the energy range 0.1 – 10 keV (observer’s frame), of four BL Lacertae objects selected from the 1 Jy sample. All sources display a flat ( $\alpha_x \sim 0.7$ ) X-ray spectrum, which we interpret as inverse Compton emission. One object shows evidence for a low-energy steepening ( $\Delta\alpha_x \sim 0.9$ ) which is likely due to the synchrotron component merging into the inverse Compton one around  $\sim 2$  keV. A variable synchrotron tail would explain why the *ROSAT* spectra of our sources are typically steeper than the *BeppoSAX* ones ( $\Delta\alpha_x \sim 0.7$ ). The broad-band spectral energy distributions fully confirm this picture and model fits using a synchrotron inverse Compton model allow us to derive the physical parameters (intrinsic power, magnetic field, etc.) of our sources. By combining the results of this paper with those previously obtained on other sources we present a detailed study of the *BeppoSAX* properties of a well-defined sub-sample of 14 X-ray bright ( $f_x(0.1 - 10 \text{ keV}) > 3 \times 10^{-12} \text{ erg cm}^{-2} \text{ s}^{-1}$ ) 1-Jy BL Lacs. We find a very tight proportionality between nearly simultaneous radio and X-ray powers for the 1-Jy sources in which the X-ray band is dominated by inverse Compton emission, which points to a strong link between X-ray and radio emission components in these objects.

**Key words:** galaxies: active – X-ray: observations

## 1 INTRODUCTION

BL Lacertae objects constitute one of the most extreme classes of active galactic nuclei (AGN), distinguished by their high luminosity, rapid variability, high ( $\gtrsim 3$  per cent) optical and radio polarization, radio core-dominance, apparent superluminal speeds, and almost complete lack of emission lines (e.g., Kollgaard 1994; Urry & Padovani 1995). The broad-band emission in these objects, which extends from the radio to the gamma-ray band, appears to be dominated by non-thermal processes from the heart of the AGN, undiluted by the thermal emission present in other AGN. Therefore, BL Lacs represent the ideal class to study to further our understanding of non-thermal emission in AGN.

Synchrotron emission combined with inverse Compton scattering is generally thought to be the mechanism respon-

sible for the production of radiation over such a wide energy range (e.g., Ghisellini et al. 1998). The synchrotron peak frequency,  $\nu_{\text{peak}}$ , ranges across several orders of magnitude, going from the far-infrared to the hard X-ray band. Sources at the extremes of this wide distribution are referred to as low-energy peaked (LBL) and high-energy peaked (HBL) BL Lacs, respectively (Giommi & Padovani 1994; Padovani & Giommi 1995). Radio-selected samples include mostly objects of the LBL type, while X-ray selected samples are mostly made up of HBL.

This scenario makes clear and strong predictions on the X-ray spectra for the two classes. In the relatively narrow *ROSAT* band differences between the two classes became apparent only when very large BL Lac samples ( $\sim 50$  per cent of the then known objects) were considered (Padovani & Giommi 1996; Lamer, Brunner & Staubert 1996). The *BeppoSAX* satellite with its broad-band X-ray (0.1 – 200 keV) spectral capabilities, is particularly well suited for a

\* Email: padovani@stsci.edu

arXiv:astro-ph/0311084v1 4 Nov 2003

detailed analysis of the individual X-ray spectra of these sources.

In Padovani et al. (2001; Paper I) we presented *BeppoSAX* observations of seven 1-Jy BL Lacs (plus an additional “intermediate” source), six of them LBL. We discuss here *BeppoSAX* observations of four additional 1-Jy BL Lacs, all of the LBL type.

In Section 2 we present our sample, Section 3 discusses the observations and the data analysis, while Section 4 describes the results of our spectral fits to the *BeppoSAX* data. Section 5 deals with the *ROSAT* data for our sources, while Section 6 presents the spectral energy distributions. Section 7 discusses the X-ray properties of all 1-Jy BL Lacs observed by *BeppoSAX*, while Section 8 presents our conclusions.

Throughout this paper spectral indices are written  $S_\nu \propto \nu^{-\alpha}$  and the values  $H_0 = 50 \text{ km s}^{-1} \text{ Mpc}^{-1}$  and  $q_0 = 0$  have been adopted.

## 2 THE SAMPLE

The 1-Jy sample of BL Lacs is presently the only sizeable, complete sample of radio bright BL Lacs. It includes 34 objects with radio flux  $> 1 \text{ Jy}$  at 5 GHz and  $\alpha_r \leq 0.5$  (Stickel et al. 1991). All 1-Jy BL Lacs have been studied in detail in the radio and optical bands; all objects have also soft X-ray data, primarily from *ROSAT*.

We selected for *BeppoSAX* observations all 1-Jy BL Lacs with 0.1 – 10 keV X-ray flux larger than  $2 \times 10^{-12} \text{ erg cm}^{-2} \text{ s}^{-1}$  (estimated from an extrapolation of the single power-law fits derived for these objects from *ROSAT* data; Urry et al. 1996). This included twenty 1-Jy BL Lacs (or  $\sim 60$  per cent of the sample). Observing time was granted for 11 of them, while three more sources have been included in other *BeppoSAX* programs (MKN 501: Pian et al. 1998; S5 0716+714: Giommi et al. 1999; PKS 0537–441: Pian et al. 2002). We present here the results obtained for the four objects observed in Cycle 2, all LBL. The object list and basic characteristics are given in Table 1, which presents the source name, position, redshift,  $R$  magnitude, 5 GHz radio flux, and Galactic  $N_{\text{H}}$ .

## 3 OBSERVATIONS AND DATA ANALYSIS

A complete description of the *BeppoSAX* mission is given by Boella et al. (1997a). The relevant instruments for our observations are the coaligned Narrow Field Instruments (NFI), which include one Low Energy Concentrator Spectrometer (LECS; Parmar et al. 1997) sensitive in the 0.1 – 10 keV band; two (three before 1997 May) identical Medium Energy Concentrator Spectrometers (MECS; Boella et al. 1997b), covering the 1.5 – 10 keV band; and the Phoswich Detector System (PDS; Frontera et al. 1997), coaligned with the LECS and the MECS. The PDS instrument is made up of four units, and was operated in collimator rocking mode, with a pair of units pointing at the source and the other pair pointing at the background, the two pairs switching on and off source every 96 seconds. The net source spectra have been obtained by subtracting the ‘off’ to the ‘on’ counts. A journal of the observations is given in Table 2.

The data analysis was based on the linearized, cleaned

event files obtained from the *BeppoSAX* Science Data Center (SDC) on-line archive (Giommi & Fiore 1997). The data from the two MECS instruments were merged in one single event file by the SDC, based on sky coordinates. The event file was then screened with a time filter given by SDC to exclude those intervals related to events without attitude solution (i.e., conversion from detector to sky coordinates; see Fiore et al. 1999). This was done to avoid an artificial decrease in the flux. As recommended by the SDC, the channels 1–10 and above 4 keV for the LECS and 0–36 and 220–256 for the MECS were excluded from the spectral analysis, due to residual calibration uncertainties. None of our sources was detected by the PDS.

Spectra and lightcurves were extracted using the standard radius of 4 arcmin for the MECS. As regards the LECS, the recommended value of 8 arcmin was used only for S5 1803+784, while 6 and 4 arcmin were used for AO 0235+164 and OQ 530, respectively, due to their very low signal-to-noise ratio (S/N). A 4 arcmin radius was used for 3C 371, due to the presence of a serendipitous source at  $\sim 7$  arcmin (see below).

The spectral analysis was performed using the matrices and blank-sky background files released in 1998 November by the SDC, with the blank-sky files extracted in the same coordinate frame as the source file, as described in Paper I. Because of the importance of the band below 1 keV to assess the presence of extra absorption or soft excess (indicative of a low-energy steepening of the spectrum), we have also checked the LECS data for differences in the cosmic background between local and blank-sky field observations, comparing spectra extracted from the same areas on the detector (namely, two circular regions outside the 10 arcmin radius central region, located at the opposite corners with respect to the two on-board radioactive calibration sources). No significant differences were found.

Using the software package XRONOS we looked for time variability in every observation, binning the data in intervals from 500 to 3600 s, with null results.

## 4 SPECTRAL FITS

Spectral analysis has been performed with the XSPEC 10.00 package, using the response matrices released by the SDC in 1998. Using the program GRPPHA, the spectra were rebinned with more than 20 counts in every new bin and using the rebinning files provided by SDC. Various checks using different rebinning strategies have shown that our results are independent of the adopted rebinning within the uncertainties. The data were analyzed applying the Gehrels statistical weight (Gehrels 1986) in case the resulting net counts were below 20 (typically 12–15 in the low energy band of LECS). The LECS/MECS normalization factor was left free to vary in the range 0.65–1.0, as suggested by SDC (see Fiore et al. 1999). The X-ray spectra of our sources are shown in Fig. 1.

### 4.1 Single Power-law Fits

At first, we fitted the combined LECS and MECS data with a single power-law model with Galactic and free absorption. The absorbing column was parameterized in terms of  $N_{\text{H}}$ , the HI column density, with heavier elements fixed at solar

**Table 1.** Sample Properties.

Name	RA(J2000)	Dec(J2000)	$z$	$R_{\text{mag}}^a$	$F_{5\text{GHz}}$ (Jy)	Galactic $N_{\text{H}}$ ( $10^{20} \text{ cm}^{-2}$ )
AO 0235+164	02 38 38.9	+16 36 59	0.940	16.5	2.9	7.60 <sup>b</sup>
OQ 530	14 19 46.6	+54 23 15	0.152	14.5	1.1	1.20 <sup>c</sup>
S5 1803+784	18 00 45.7	+78 28 04	0.684	16.5	2.6	3.65 <sup>d</sup>
3C 371	18 06 50.6	+69 49 28	0.051	14.0	2.3	4.38 <sup>d</sup>

<sup>a</sup> Mean R magnitude from Heidt & Wagner (1996).

<sup>b</sup> From Elvis et al. (1989).

<sup>c</sup> Dickey & Lockman (1990).

<sup>d</sup> From Murphy et al. (1996).

**Table 2.** BeppoSAX Journal of observations.

Name	LECS	LECS	MECS	MECS	Observing date
	Exp. (s)	Count rate <sup>a</sup> (cts/s)	Exp. (s)	Count rate <sup>a</sup> (cts/s)	
AO 0235+164	24575	0.006 ± 0.002	29071	0.011 ± 0.001	1999 Jan 28
OQ 530	16312	0.006 ± 0.002	39680	0.008 ± 0.001	1999 Feb 12-13
S5 1803+784	18359	0.013 ± 0.002	40303	0.028 ± 0.001	1998 Sep 28
3C 371	13090	0.018 ± 0.002	33760	0.024 ± 0.001	1998 Sep 22-23

<sup>a</sup> Net count rate full band.

abundances and cross sections taken from Morrison and Mc-Cammon (1983). The  $N_{\text{H}}$  value for AO 0235+164 was also fixed at a value larger than the Galactic one to take into account absorption by an intervening galaxy (Madejski et al. 1996).  $N_{\text{H}}$  was also set free to vary for all sources to check for internal absorption and/or indications of a “soft-excess.”

Our results are presented in Table 3, which gives the name of the source in column (1),  $N_{\text{H}}$  in column (2), the energy index  $\alpha_{\text{x}}$  in column (3), the 1 keV flux in  $\mu\text{Jy}$  in column (4), the unabsorbed 2 – 10 keV and 0.1 – 2.4 keV fluxes in columns (5)-(6), the LECS/MECS normalization in column (7), the reduced chi-square and number of degrees of freedom,  $\chi^2_{\nu}/(\text{dof})$  in column (8), and the  $F$ -test probability that the decrease in  $\chi^2$  due to the addition of a new parameter (free  $N_{\text{H}}$ ) is significant in column (9). The errors quoted on the fit parameters are the 90 per cent uncertainties for one and two interesting parameters, for Galactic and free  $N_{\text{H}}$  respectively. The errors on the 1 keV flux reflect the statistical errors only and not the model uncertainties.

Two results are immediately apparent from Table 3. First, the fitted  $N_{\text{H}}$  values do not agree with the Galactic ones for AO 0235+164 (as expected from previous ASCA and *ROSAT* observations; see Sect. 4.2.1) and possibly OQ 530. An  $F$ -test shows that the addition of  $N_{\text{H}}$  as a free parameter results in a (marginally significant) improvement in the  $\chi^2$  values only for AO 0235+164 (column 9 of Table 3). Second, the fitted energy indices are flat,  $\alpha_{\text{x}} < 1$ , with  $\langle \alpha_{\text{x}} \rangle = 0.67 \pm 0.11$  and a weighted mean equal to  $0.59 \pm 0.09$ .

One of our sources, OQ 530, appears to show a low-energy excess, as illustrated by Fig. 1 and by the fact that the best fit  $N_{\text{H}}$  in Table 3 is below the Galactic value (and actually consistent with zero). We then fitted a broken power-law model to the data. The results are presented in Table 4, which gives the name of the source in column (1),  $N_{\text{H}}$  in column (2), the soft energy index  $\alpha_{\text{S}}$  in column (3), the hard energy index  $\alpha_{\text{H}}$  in column (4), the break energy in column

(5), the 1 keV flux in  $\mu\text{Jy}$  in column (6), the unabsorbed 2 – 10 keV and 0.1 – 2.4 keV fluxes in columns (7)-(8), the LECS/MECS normalization in column (9), the reduced chi-squared and number of degrees of freedom,  $\chi^2_{\nu}/(\text{dof})$ , in column (10), and the  $F$ -test probability that the decrease in  $\chi^2$  due to the addition of two parameters (from a single power-law fit to a broken power-law fit) is significant in column (11). Although the fit is improved by using a double power-law model, an  $F$ -test shows that the improvement is more suggestive than significant, with a probability  $\sim 90$  per cent. The best-fit spectrum, however, points in the direction of a flatter component emerging at higher energies, as was the case for four sources in Paper I. In fact, the spectrum is concave with a large spectral change  $\langle \alpha_{\text{S}} - \alpha_{\text{H}} \rangle \sim 0.9$ , and an energy break around  $E \sim 2$  keV. Evidence for a concave spectrum comes also from the shape of the ratio of the data to the single power-law fits, shown in Fig. 1.

## 4.2 Notes on individual sources

### 4.2.1 AO 0235+164

This source is in a crowded field, with three absorbing systems at  $z = 0.524$ , 0.851, and 0.94 in a  $10 \times 10$  arcsec region and a probable Seyfert 1 galaxy at less than 5 arcsec (see Burbidge et al. 1996). *ROSAT* and ASCA spectra show absorption above the Galactic value, which our data confirm, likely due to the intervening absorption system at  $z = 0.524$  (Madejski et al. 1996). A fit with free absorption, in fact, gives an  $N_{\text{H}}$  value slightly higher than the corresponding ASCA one ( $3.7 \times 10^{21} \text{ cm}^{-2}$  vs.  $2.8 \times 10^{21} \text{ cm}^{-2}$ ) but still consistent within the errors. Since the ASCA data provide a better constraint on the column density, we have also fitted our data with total  $N_{\text{H}}$  fixed at the ASCA value. The *BeppoSAX* X-ray spectral index and flux are consistent with

**Table 3.** Single power-law fits, LECS + MECS<sup>a</sup>.

Name	$N_H$ ( $10^{20}$ cm <sup>-2</sup> )	$\alpha_x$	$F_{1keV}$ ( $\mu$ Jy)	$F_{[2-10]}$ (c.g.s.)	$F_{[0.1-2.4]}$ (c.g.s.)	Norm (L/M)	$\chi^2_\nu/\text{dof}$	$F$ -test, notes fixed-free $N_H$
AO 0235+164	7.6 fixed	$0.79^{+0.24}_{-0.24}$	$0.16^{+0.06}_{-0.05}$	8.54e-13	1.08e-12	0.70	0.97/14	
	$37^{+85}_{-33}$	$1.01^{+0.47}_{-0.41}$	$0.22^{+0.16}_{-0.08}$	8.43e-13	1.71e-12	0.82	0.78/13	94 per cent
	28 <sup>b</sup> fixed	$0.96^{+0.27}_{-0.26}$	$0.20^{+0.08}_{-0.06}$	8.42e-13	1.51e-12	0.79	0.74/14	$N_H$ at ASCA and ROSAT values
OQ 530	1.20 fixed	$0.55^{+0.27}_{-0.32}$	$0.09^{+0.03}_{-0.03}$	6.74e-13	5.24e-13	0.74	1.12/15	
	0.0(< 7.38)	$0.55^{+0.32}_{-0.39}$	$0.09^{+0.03}_{-0.03}$	6.75e-13	5.24e-13	0.71	1.09/14	74 per cent
S5 1803+784	3.65 fixed	$0.45^{+0.12}_{-0.12}$	$0.24^{+0.04}_{-0.04}$	2.21e-12	1.41e-12	0.67	0.97/22	
	10(< 33)	$0.51^{+0.20}_{-0.20}$	$0.26^{+0.07}_{-0.05}$	2.20e-12	1.57e-12	0.67	0.97/21	65 per cent
3C 371	4.38 fixed	$0.72^{+0.16}_{-0.16}$	$0.30^{+0.07}_{-0.07}$	1.76e-12	1.93e-12	0.72	0.86/30	
	$5.6^{+19}_{-4.6}$	$0.74^{+0.24}_{-0.24}$	$0.30^{+0.08}_{-0.08}$	1.76e-12	1.99e-12	0.73	0.89/29	30 per cent

<sup>a</sup>Errors are at 90 per cent confidence level for one (with fixed  $N_H$ ) and two parameters of interest.

<sup>b</sup>Absorption including the contribution of an intervening system at  $z=0.524$  (Madejski et al. 1996).

**Table 4.** Broken power-law fits, LECS + MECS<sup>a</sup>.

Name	$N_H$ ( $10^{20}$ cm <sup>-2</sup> )	$\alpha_S$	$\alpha_H$	$E_{break}$ (keV)	$F_{1keV}$ ( $\mu$ Jy)	$F_{[2-10]}$ (c.g.s.)	$F_{[0.1-2.4]}$ (c.g.s.)	L/M	$\chi^2_\nu/\text{dof}$	$F$ -test <sup>b</sup>
OQ 530	1.20 fixed	$1.3^{+4.0}_{-0.7}$	$0.4^{+0.4}_{-0.4}$	$1.8^{+1.1}_{-1.5}$	$0.12^{+0.03}_{-0.07}$	7.31e-13	1.10e-12	0.66	0.91/13	90 per cent

<sup>a</sup>Errors are at 90 per cent confidence level for two parameters of interest.

<sup>b</sup>The values of the  $F$ -test refer to the comparison with a single power-law model with Galactic column density.

the values of Madejski et al. (1996), under the same assumptions.

Given the *BeppoSAX* point spread function, it is nearly impossible to assess the likelihood of a contribution from the Seyfert galaxy to the X-ray flux of our source. However, the MECS profile is the one expected from a point-like source, with no hints of extension. Moreover, using its observed optical magnitude ( $\sim 20.5$ ) and assuming an optical-X-ray effective spectral index typical of Seyfert 1s ( $\alpha_{ox} \sim 1.2$ ), one can estimate an X-ray flux from this nearby source roughly a factor of 10 smaller than that observed for AO 0235+164.

#### 4.2.2 OQ 530

This source shows some evidence of a steeper spectrum at low energies, but the  $F$ -test significance is only marginal, due to the low statistics and narrow range affected. Tagliarferri et al. (2003) have also presented evidence for a low-energy excess, with a very steep  $\alpha_S \sim 6.7$  and  $\alpha_H = 0.4 \pm 0.2$  (2000 March 3-4) and  $\alpha_H = 0.75 \pm 0.20$  (2000 March 26-27). In their case the  $F$ -test probability for improvement for the double power-law model is  $> 99.9$  per cent and  $\sim 80$  per cent, respectively. The fluxes for the two observations are similar,  $f(2 - 10\text{keV}) \sim 10^{-12}$  erg cm<sup>-2</sup> s<sup>-1</sup>,  $\sim 50$  per cent larger than what we find.

#### 4.2.3 3C 371

A serendipitous source identified as RIXOS F272\_023, a Seyfert 1.8 galaxy at  $z = 0.096$ , is present in the LECS and MECS images, at a distance of  $\sim 7$  arcmin (Puchnarewicz et al. 1997). The extraction of LECS data was then done by using a radius of 4 arcmin.

## 5 ROSAT PSPC DATA

In order to compare our results with previous (soft) X-ray observations and especially to take advantage of the higher resolution and collecting area at low energies, we used data from the ROSAT Position Sensitive Proportional Counter (PSPC). The 1-Jy BL Lac ROSAT data had been originally published by Urry et al. (1996). In order to ensure a uniform procedure for the whole sample, we have re-analyzed all ROSAT data, obtaining results consistent within the errors with those already published.

The journal of the ROSAT observations is given in Table 5. The basic event files from the archive have been corrected for gain variations on the detector surface with the program PCSASSCORR in FTOOLS, when not already done by the Standard Reduction process (SASS version 7.2.8 and later, M. Corcoran, private communication). Since all the sources were ROSAT targets a standard extraction radius of 3' (2.5' when serendipitous sources were present in the field or when the source was particularly weak) was used, to avoid the

**Table 5.** *ROSAT* journal of observations.

Name	Exposure (s)	Full band net countrate (cts/s)	Observing Date
AO 0235+164	17949	$0.170 \pm 0.003$	1993 Jul 21 – Aug 15
OQ 530	11474	$0.223 \pm 0.005$	1990 Jul 19 – 23
S5 1803+784	6781	$0.081 \pm 0.004$	1992 Apr 7
	2773	$0.105 \pm 0.008$	1992 Jul 25
	2827	$0.108 \pm 0.008$	1992 Dec 10
3C 371	10348	$0.127 \pm 0.004$	1992 Apr 9

possible loss of soft photons due to the ghost imaging effect. We have used the appropriate response matrices for the different gain levels of the PSPC B detector before and after 14 Oct. 1991 (gain1 and gain2, respectively). The background has been evaluated in two circular regions (of radius  $\sim 20 - 30$  pixels) away from the central region and from other serendipitous sources, but inside the central rib of the detector. The spectra have been rebinned (using GRPPHA) with more than 20 counts in every new bin, to validate the use of  $\chi^2$  statistics. Channel 1-11 and 212-256 have been excluded from the analysis, due to calibration uncertainties.

As for the *BeppoSAX* data, we fitted the *ROSAT* PSPC data with a single power-law model with Galactic and free absorption. Our results are presented in Table 6, which gives the name of the source in column (1),  $N_{\text{H}}$  in column (2), the energy index  $\alpha_{\text{x}}$  in column (3), the 1 keV flux in  $\mu\text{Jy}$  in column (4), the unabsorbed 0.1–2.4 keV flux in column (5), the reduced chi-squared and number of degrees of freedom,  $\chi^2_{\nu}/(\text{dof})$  in column (6), and the observing date in column (7).

Table 6 shows that the fitted  $N_{\text{H}}$  values are consistent with the Galactic ones for OQ 530 and S5 1803+784. AO 0235+164 shows evidence of excess absorption, as was the case for our *BeppoSAX* data, while 3C 371 displays a soft-excess, suggestive of a steeper soft component. A broken power-law fit, in fact, improves the fit significantly (99.7 per cent), as shown in Table 7. The spectrum is obviously concave with quite a large spectral change, with  $\langle\alpha_{\text{S}} - \alpha_{\text{H}}\rangle \sim 2$ , and an energy break around  $E \sim 0.3$  keV.

The fitted energy indices are relatively steep. The mean *ROSAT* value for our sources is  $\langle\alpha_{\text{x}}\rangle = 1.34 \pm 0.18$ , while the weighted mean is  $\langle\alpha_{\text{x}}\rangle = 1.21 \pm 0.04$ .

## 5.1 Notes on individual sources

### 5.1.1 AO 0235+164

Nine *ROSAT* observations are available, spaced by about  $\sim 3$  days, between July 21 and August 15 1993. The source shows some interesting variability, but with no evident spectral variations, as the hardness ratio is roughly constant. Therefore, the data have been summed together (see Madejski et al. 1996 for a discussion of the single observations).

### 5.1.2 OQ 530

The *ROSAT* observations are relatively old and done with the PSPC C detector. The spectrum has many "wiggles", which suggest that perhaps the calibration is not optimal.

The resulting reduced  $\chi^2$  is not very good, but alternative models (free  $N_{\text{H}}$ , broken power-law) do not improve the fit.

### 5.1.3 S5 1803+784

Three *ROSAT* observations are available. The best-fit  $N_{\text{H}}$  agrees with the Galactic value. The source displays interesting spectral and intensity variations, with a "steeper when brighter" behaviour, which suggests properties typical of "intermediate" BL Lacs. These are possibly associated with a shift of the synchrotron peak or a hardening of the injected electron spectrum in higher states, so that synchrotron emission becomes dominant in the soft X-ray band.

## 5.2 Comparison between *BeppoSAX* and *ROSAT* results

Figure 2 shows the 0.1–2.4 keV *BeppoSAX* flux versus the corresponding *ROSAT* flux. Our sources display mild X-ray variability: the median value of  $f_{\text{BeppoSAX}}/f_{\text{ROSAT}}$  is 0.4. Fig. 2 includes also the BL Lacs studied in Paper I. Most sources have  $f_{\text{BeppoSAX}} < f_{\text{ROSAT}}$ , as shown by the fact that the median value for all 12 sources is  $f_{\text{BeppoSAX}}/f_{\text{ROSAT}}$  is 0.4. Fig. 2 should be compared with Fig. 2 of Wolter et al. (1998; see also Beckmann et al. 2002), which plots the *BeppoSAX* 1 keV fluxes versus the corresponding *ROSAT* fluxes for a sample of 8 HBL. There the two fluxes are within 30 per cent for most sources and the points follow more closely the line of equal fluxes. Note that the median value of the flux ratio at 1 keV is  $\sim 0.5$  for the 4 sources studied in this paper (and  $\sim 0.6$  if one includes those studied in Paper I).

Figure 3 shows the *BeppoSAX* spectral index (0.1–10 keV) vs. the *ROSAT* spectral index (0.1–2.4 keV). The larger *BeppoSAX* error bars for most of our sources, as compared to *ROSAT*, are due to the worse photon statistics. (The PSPC count rates, in fact, are typically a factor of 20 larger than the LECS ones.) All sources studied in this paper occupy the region of the plot where  $\alpha_{\text{x}}(\text{BeppoSAX}) < \alpha_{\text{x}}(\text{ROSAT})$ . The interpretation of this plot is complicated by variability effects, which affect the shape of the X-ray spectrum, and possibly by *ROSAT* miscalibrations (e.g., Iwasawa, Fabian & Nandra 1999). Keeping this in mind, in agreement with our previous results the figure suggests a concave overall X-ray spectrum for our sources, with a flatter component emerging at higher energies. We find  $\alpha_{\text{x}}(\text{ROSAT}) - \alpha_{\text{x}}(\text{BeppoSAX}) = 0.7 \pm 0.1$ . This difference can hardly be explained by miscalibration effects which, if present, should only steepen the *ROSAT* slopes

**Table 6.** *ROSAT* PSPC, single power-law fits<sup>a</sup>.

Name	$N_{\text{H}}$ ( $10^{20}$ cm $^{-2}$ )	$\alpha_x$	$F_{1\text{keV}}$ ( $\mu\text{Jy}$ )	$F_{[0.1-2.4]}$ (erg cm $^{-2}$ s $^{-1}$ )	$\chi^2/\text{dof}$	Observing Date
AO 0235+164	7.60 fixed	$0.50 \pm 0.08$	$0.64 \pm 0.02$	3.84e-12	3.22/30	1993 Jul 21 – Aug 15
	$33_{-10}^{+12}$	$2.1 \pm 0.7$	$1.4_{-0.3}^{+0.4}$	4.45e-11	0.79/29	
	$28^b$ fixed	$1.88 \pm 0.11$	$1.21 \pm 0.04$	2.37e-11	0.79/30	
OQ 530 <sup>c</sup>	1.20 fixed	$1.07 \pm 0.05$	$0.30 \pm 0.02$	2.47e-12	1.32/76	1990 Jul 19 – 23
	$1.2_{-0.3}^{+0.4}$	$1.1 \pm 0.2$	$0.30 \pm 0.02$	2.50e-12	1.34/75	
S5 1803+784	3.65 fixed	$0.84 \pm 0.15$	$0.23 \pm 0.02$	1.61e-12	0.89/21	1992 Apr 7
	$4.2_{-1.6}^{+1.9}$	$1.0 \pm 0.4$	$0.24 \pm 0.02$	1.79e-12	0.91/20	
	3.65 fixed	$1.2 \pm 0.2$	$0.27 \pm 0.03$	2.40e-12	0.68/10	1992 Jul 25
	$3.5_{-2.0}^{+2.4}$	$1.1 \pm 0.7$	$0.27 \pm 0.04$	2.28e-12	0.76/9	
	3.65 fixed	$1.2 \pm 0.2$	$0.26 \pm 0.03$	2.38e-12	1.32/10	1992 Dec 10
	$4.6_{-2.4}^{+2.8}$	$1.5 \pm 0.8$	$0.26 \pm 0.04$	3.20e-12	1.40/9	
3C 371	4.38 fixed	$1.21 \pm 0.10$	$0.35 \pm 0.02$	3.20e-12	1.36/25	1992 Apr 9
	$2.7_{-0.8}^{+0.9}$	$0.8 \pm 0.3$	$0.33 \pm 0.02$	2.21e-12	0.85/24	

<sup>a</sup>Errors are at 90 per cent confidence level for one (with fixed  $N_{\text{H}}$ ) and two parameters of interest.

<sup>b</sup>Absorption including the contribution of an intervening system at  $z=0.524$  (Madejski et al. 1996).

<sup>c</sup>PSPC C

**Table 7.** Broken power-law fits, *ROSAT*<sup>a</sup>.

Name	$N_{\text{H}}$ ( $10^{20}$ cm $^{-2}$ )	$\alpha_S$	$\alpha_H$	$E_{\text{break}}$ (keV)	$F_{1\text{keV}}$ ( $\mu\text{Jy}$ )	$F_{[0.1-2.4]}$ (c.g.s.)	$\chi^2/\text{dof}$	$F$ -test <sup>b</sup>
3C 371	4.38 fixed	$3.0_{-2.2}^{+2.4}$	$0.9 \pm 0.2$	$0.34_{-0.06}^{+0.64}$	$0.3 \pm 0.1$	5.60e-12	0.88/23	99.7 per cent

<sup>a</sup>Errors are at 90 per cent confidence level for two parameters of interest.

<sup>b</sup>The values of the  $F$ -test refer to the comparison with a single power-law model with Galactic column density.

by  $\sim 0.2 - 0.3$  (see also Mineo et al. 2000). Fig. 3 includes also the BL Lacs studied in Paper I. Note that only one BL Lac has  $\alpha_x(\text{ROSAT}) < \alpha_x(\text{BeppoSAX})$  and that for all 12 sources we find  $\alpha_x(\text{ROSAT}) - \alpha_x(\text{BeppoSAX}) = 0.53 \pm 0.16$  ( $0.53 \pm 0.18$  excluding the two HBL).

Again, this figure should be compared with Fig. 3 of Wolter et al. (1998), which shows the same plot for a sample of 8 HBL. In that case the *BeppoSAX* and *ROSAT* spectral indices agree within the errors for all but one source. A sample of 10 HBL studied by Beckmann et al. (2002) shows more scatter but the mean values for the spectral indices are still similar.

Looking at the differences between *BeppoSAX* and *ROSAT* spectra in more detail, OQ 530 shows, as discussed above (see Tab. 4), evidence of a steeper *BeppoSAX* spectrum at low energies (very significant for the data presented by Tagliaferri et al. 2003), consistent with the *ROSAT* data. Similarly, the *ROSAT* spectrum of 3C 371 is best fitted by a broken power-law with a hard component consistent with the *BeppoSAX* spectrum and a steep, soft component which dominates only for  $E \lesssim 0.3$  keV. Could a *ROSAT*-

like component be also present in the *BeppoSAX* spectra of our other two sources but not have been detected? The answer is: no. We have simulated this by assuming a broken power-law model with a break at 2.4 keV (the end of the *ROSAT* band) and a hard component with spectral index equal to that measured by *BeppoSAX*. A soft component with spectral index equal to that seen by *ROSAT* can be excluded with very strong significance ( $> 99$  per cent) for both AO 0235+164 and S5 1803+784. If the flux were also constrained to be the same as the *ROSAT* one the significance of the exclusion would be even higher. In other words, *BeppoSAX* did not detect a steep, *ROSAT*-like component in these two sources because it was not there.

## 6 SPECTRAL ENERGY DISTRIBUTIONS

To address the relevance of our *BeppoSAX* data in terms of emission processes in BL Lacs, we have assembled multifrequency data for all our sources. The main source of information was NED, and so most data are not simultaneous with our *BeppoSAX* observations. For all our sources, however,

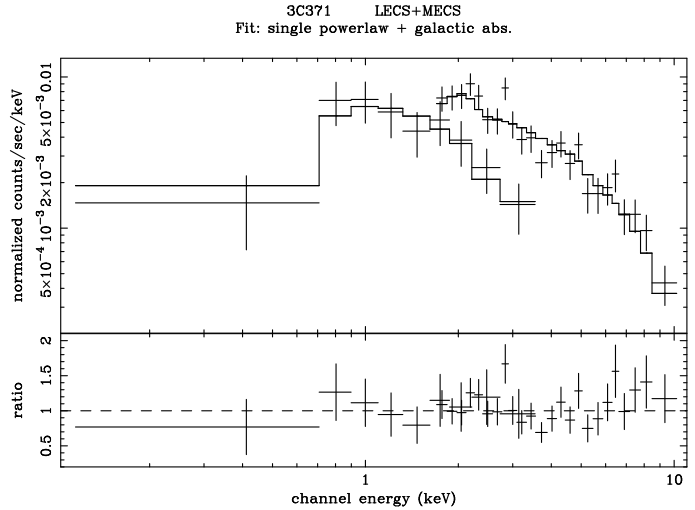
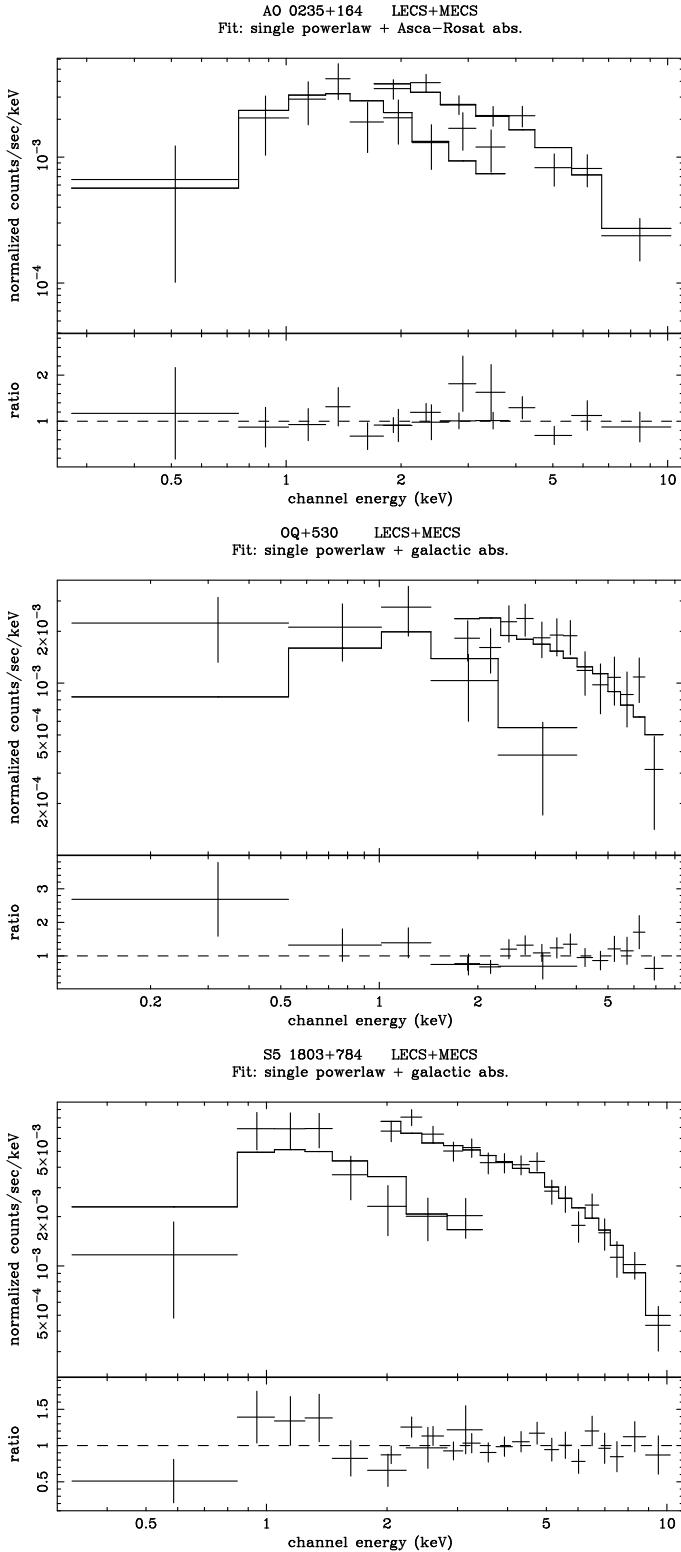


**Figure 1.** *BeppoSAX* data and fitted spectra for our sources, and ratio of data to fit. Data are from the LECS and MECS instruments. The data are fitted with a single power-law model with Galactic absorption, apart from AO 0235+164, for which the absorption includes also the contribution of an intervening system at  $z = 0.524$  (Madejski et al. 1996).

8.0 GHz derived from the UMRAO data. One of our sources (AO 0235+164) has been detected by EGRET so its energy distribution reaches  $\sim 5 \times 10^{24}$  Hz. The EGRET data come from the compilation of Lin et al. (1999), which include the first entries in the Third EGRET Catalog.

The spectral energy distributions (SEDs) for our sources are shown in Fig. 4, where filled circles indicate *BeppoSAX* data and the nearly-simultaneous radio data, and open symbols represent non-simultaneous literature (mostly NED) data. The *BeppoSAX* data have been converted to  $\nu f_\nu$  units using the XSPEC unfolded spectra after correcting for absorption. *ROSAT* (from Tab. 6 and 7) and EGRET data are shown by a bow-tie that represents the spectral index range. The plotted *ROSAT* data correspond to the fixed galactic column density fits (for AO 0235+164 the one including the extra absorption), and to the highest and lowest flux observed. For 3C 371, we plotted the spectral index range from the broken power-law fits (above 0.3 keV; Tab. 7). We also show the available ASCA data for AO 0235+164 (Madejski et al. 1996) and 3C 371 (Donato et al. 2001).

To derive the intrinsic physical parameters that could account for the observed data, we have fitted the SED of our sources with an homogeneous, one-zone synchrotron inverse Compton model as developed in Ghisellini, Celotti & Costamante (2002). This model is very similar to the one described in detail in Spada et al. (2001; it is the “one-zone” version of it), and is characterized by a finite injection timescale, of the order of the light crossing time of the emitting region (as occurs, for example, in the internal shocks scenario, where the dissipation takes place during the collision of two shells of fluid moving at different speeds).

In this model, the main emission comes from a single zone and a single population of electrons, with the particle energy distribution determined at the time  $t_{\text{inj}}$ , i.e., at the end of the injection, which is the time when the emitted luminosity is maximized. Details of the model can be found

we were able to find nearly-simultaneous (typically within a month) radio observations in the University of Michigan Radio Astronomy Observatory (UMRAO) database. These are reported in Table 8, which also gives the nearly-simultaneous radio-X-ray spectral index,  $\alpha_{\text{rx}}$  with its error. This is defined between the rest-frame frequencies of 4.8 GHz and 1 keV, and has been K-corrected using the X-ray spectral indices given in Tab. 3 and radio spectral indices between 4.8 and

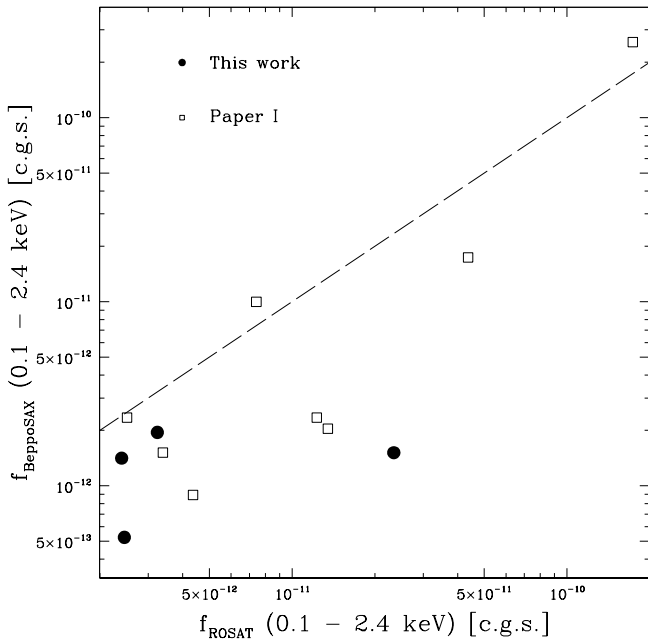


**Figure 2.** The 0.1–2.4 keV X-ray flux from our *BeppoSAX* data vs. the corresponding *ROSAT* flux (filled points). The dashed line represents the locus of  $f_{\text{BeppoSAX}} = f_{\text{ROSAT}}$ . For S5 1803+784, which has multiple *ROSAT* observations, we took the observation with the largest X-ray flux (1992 July). Open squares represent the BL Lacs studied in Paper I.

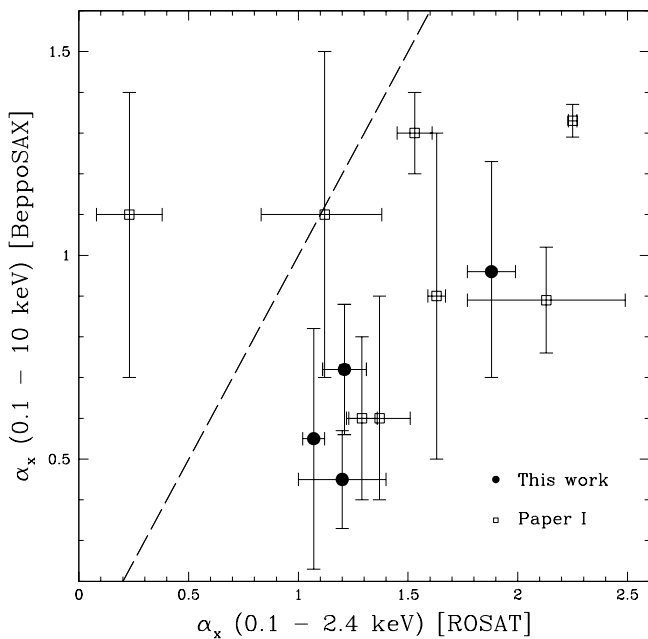


**Figure 3.** The *BeppoSAX* spectral index (0.1–10 keV) vs. the *ROSAT* spectral index (0.1–2.4 keV) for our sources (filled points). The dashed line represents the locus of  $\alpha_x(\text{BeppoSAX}) = \alpha_x(\text{ROSAT})$ . For S5 1803+784, which has multiple *ROSAT* observations, we took the observation with the largest X-ray flux (1992 July). Open squares represent the BL Lacs studied in Paper I.

in Ghisellini et al. (2002), who have applied it successfully to both low-power, high-peaked BL Lacs and powerful flat-spectrum radio quasars. A summary of the model main characteristics and a discussion of its application to the SEDs of other *BeppoSAX* sources can also be found in Padovani et al. (2001; 2002).

Some of our sources have (weak) broad lines and therefore the contribution of the disc to the SED might not be completely negligible. Furthermore, photons produced in the broad line region could contribute to the seed photon distribution for the inverse Compton scattering. We accounted for this by assuming that a fraction  $\sim 10\%$  of the disc luminosity  $L_{\text{disc}}$  is reprocessed into line emission by the broad line region (BLR),  $L_{\text{BLR}}$ , assumed to be located at  $R_{\text{BLR}}$ .  $L_{\text{BLR}}$  estimates for three of our sources were found in Celotti et al. (1997).  $R_{\text{BLR}}$  was assumed to scale as  $L_{\text{disc}}^{0.7}$ , following Kaspi et al. (2000) and disc emission was assumed to be a simple black-body peaking at  $10^{15}$  Hz.

The source is assumed to emit an intrinsic luminosity  $L'$  and to be observed with the viewing angle  $\theta$ . The input parameters are listed in Table 9, which gives the name of the source in column 1,  $L'$  in column 2,  $L_{\text{disc}}$  in column 3,  $R_{\text{BLR}}$  in column 4, the magnetic field  $B$  in column 5, the size of the region  $R$  in column 6, the Lorentz factor  $\Gamma$  in column 7, the angle  $\theta$  in column 8, the slope of the particle distribution  $n$  in column 9, the minimum Lorentz factor of the injected electrons  $\gamma_{\text{min}}$  in column 10, the Lorentz factor of the electrons emitting most of the radiation  $\gamma_{\text{peak}}$  in column 11, and finally  $\nu_{\text{peak}}^{\text{syn}}$  in column 12. Note that  $\gamma_{\text{peak}}$  and  $\nu_{\text{peak}}^{\text{syn}}$  are derived quantities and not input parameters.

The model fits are shown in Fig. 4 as solid lines. The applied model is aimed at reproducing the spectrum originating in a limited part of the jet, thought to be responsible for most of the emission. This region is necessarily compact, since it must account for the fast variability shown by all blazars, especially at high frequencies. The radio emission from this compact regions is strongly self-absorbed, and the model cannot account for the observed radio flux. This explains why the radio data are systematically above the model fits in the figures. For AO 0235+164 we have also modelled a high state corresponding to the hardest EGRET spectrum, which can be accounted for by assuming also a high X-ray state (*ROSAT* data). This is not compatible (in our model) with the *BeppoSAX* data, which instead correspond to the lowest X-ray state for this source, and can be fitted well together with the low-state EGRET data, taken quasi-simultaneously with the ASCA observation (whose flux and spectrum are very similar to the *BeppoSAX* ones; Madejski et al. 1996).

As shown in Table 9, the source dimensions, magnetic field, bulk Lorentz factors, and viewing angles are quite similar for all sources. The need for external seed photons for some sources, while indicative of a broad line region, is not extremely compelling, since the disc luminosities are much smaller than those required in radio-loud quasars (see, e.g., Ghisellini et al. 1998). The main difference between sources are in the derived value of  $\gamma_{\text{peak}}$  and intrinsic luminosities.

Fig. 4 shows that the *BeppoSAX* band is dominated by inverse Compton emission for S5 1803+784 and 3C 371, while it is in between the synchrotron and inverse Compton regions for AO 0235+164 and OQ 530. These results are consistent with the *BeppoSAX* data, as discussed in Sect. 4.

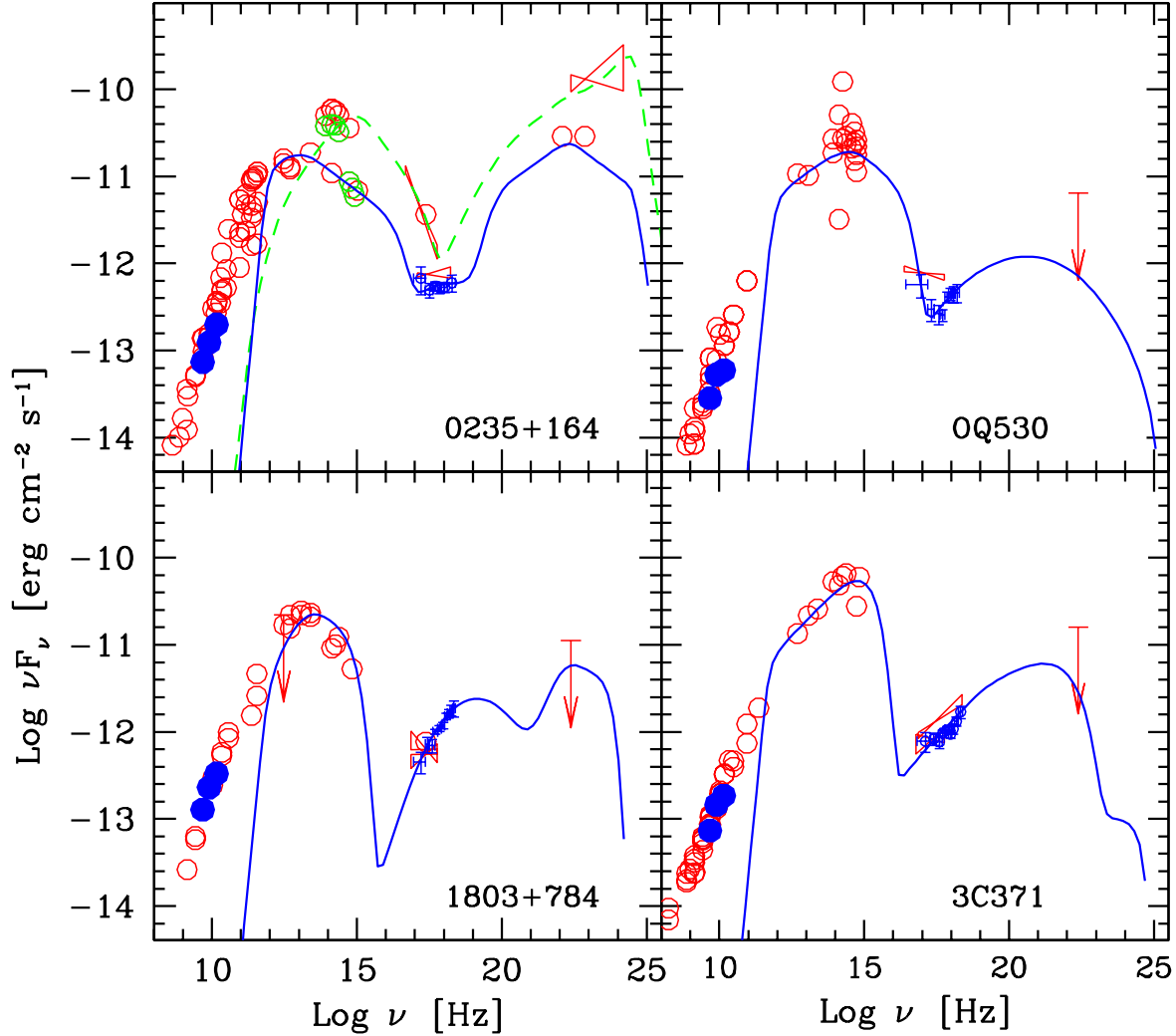


**Figure 4.** Spectral energy distributions for our sources. Filled symbols indicate *BeppoSAX* data and nearly-simultaneous radio data from UMRAO, while open symbols indicate data from NED. The solid lines correspond to the one-zone homogeneous synchrotron and inverse Compton model calculated as explained in the text, with the parameters listed in Table 9. The dashed line represents the fit to the high state of AO 0235+164. *ROSAT*, ASCA (for AO 0235+164 and 3C 371), and EGRET (high-state) data are shown by a bow-tie that represents the spectral index range.

**Table 8.** Nearly-simultaneous Radio Observations.

Name	$F_{4.8\text{GHz}}$ (Jy)	Observing date	$F_{8.0\text{GHz}}$ (Jy)	Observing date	$F_{14.5\text{GHz}}$ (Jy)	Observing date	$\alpha_{\text{rx}}$
AO 0235+164	$1.54 \pm 0.03$	1999 Jan 30	$1.55 \pm 0.08$	1999 Jan 26	$1.37 \pm 0.03$	1999 Jan 22	$0.86 \pm 0.02$
OQ 530	$0.59 \pm 0.08$	1998 Sep 24	$0.66 \pm 0.06$	1999 Feb 15	$0.41 \pm 0.01$	1999 Mar 17	$0.88 \pm 0.02$
S5 1803+784	$2.67 \pm 0.03$	1998 Sep 25	$2.88 \pm 0.17$	1998 Sep 18	$2.29 \pm 0.20$	1998 Sep 30	$0.90 \pm 0.01$
3C 371	$1.53 \pm 0.03$	1998 Sep 26	$1.82 \pm 0.18$	1998 Sep 18	$1.28 \pm 0.03$	1998 Sep 9	$0.87 \pm 0.01$

### 6.1 X-ray Spectral Index and the Synchrotron Peak Frequency

One of the aims of this project was to study the dependence of the X-ray spectral index on the synchrotron peak frequency  $\nu_{\text{peak}}$  found by Padovani & Giommi (1996) and

Lamer et al. (1996) from *ROSAT* data by using the broader *BeppoSAX* energy band. Padovani & Giommi (1996) found a strong anti-correlation between  $\alpha_{\text{x}}$  and  $\nu_{\text{peak}}$  for HBL (i.e., the higher the peak frequency, the flatter the spectrum), while basically no correlation was found for LBL. This was interpreted as due to the tail of the synchrotron compo-

**Table 9.** Model Parameters.

Name	$L'$ erg s $^{-1}$	$L_{disc}$ erg s $^{-1}$	$R_{BLR}$ cm	$B$ G	$R$ cm	$\Gamma$	$\theta$	$n$	$\gamma_{min}$	$\gamma_{peak}$	$\nu_{peak}^{syn}$ Hz
AO 0235+164	1.1e43	1.3e45	4.2e17	3.8	4.1e16	16	2.9	3.5	20	276	2.1e13
(high state)	6.3e43	1.3e45	4.2e17	1.7	2.3e16	13	2.6	3.9	3600	3600	1.5e15
OQ 530	8.0e41	...	...	3.8	1.25e16	12	4.9	3.5	70	1410	3.3e14
S5 1803+784	6.8e42	3.9e45	8.8e17	5.0	2.0e16	11	3.5	3.5	230	373	3.9e13
3C 371	2.2e41	4.8e42	1.1e16	1.8	9.0e15	13	5.0	3.3	10	5000	1.9e15

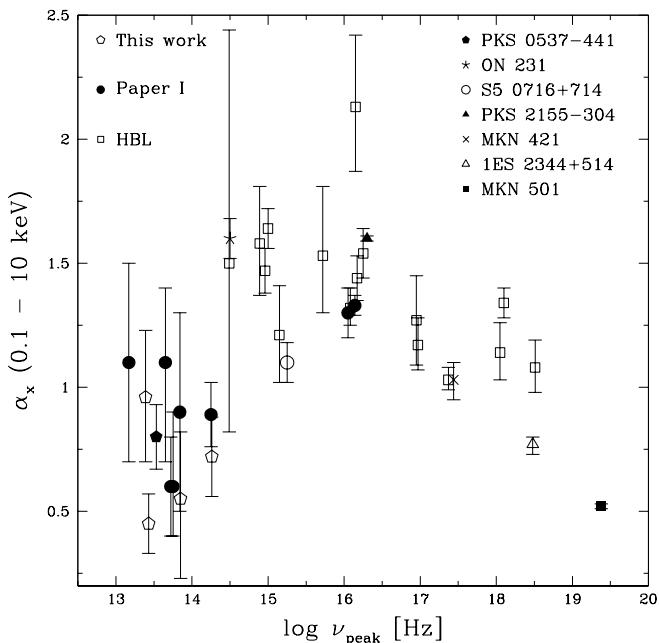


**Figure 5.** The *BeppoSAX* spectral index (0.1 – 10 keV) vs. the logarithm of the peak frequency for our sources (open pentagons), those studied in Paper I (filled circles), the HBL studied by Wolter et al. (1998) and Beckmann et al. (2002) (open squares), PKS 0537–441 (filled pentagon), ON 231 (star), S5 0716+714 (open circle), PKS 2155–304 (filled triangle), MKN 421 (cross), 1ES 2344+514 (open triangle), and MKN 501 (filled square). See text for details and references.

ment becoming increasingly dominant in the *ROSAT* band as  $\nu_{peak}$  moves closer to the X-ray band (see Fig. 7 of Padovani & Giommi 1996).

The updated *BeppoSAX* version of this dependence is shown in Fig. 5, which plots the *BeppoSAX* spectral index (0.1 – 10 keV) vs. the logarithm of the peak frequency for our sources (open pentagons), the other 1-Jy sources studied in Paper I (filled circles), the HBL studied by Wolter et al. (1998) and Beckmann et al. (2002) (open squares), and other BL Lacs studied by *BeppoSAX*. These include, in order of increasing peak frequency: PKS 0537–441 (filled pentagon; Pian et al. 2002), ON 231 (star;  $\alpha_x$  in the 0.1–3.8 keV range; Tagliaferri et al. 2000), S5 0716+714 (open circle; Giommi et al. 1999), PKS 2155–304 (filled triangle; Giommi et al. 1998), MKN 421 (cross;  $\alpha_x$  in the 0.1–1.6 keV; Fos-sati et al. 2000), 1ES 2344+514 (open triangle; Giommi, Padovani & Perlman 2000), and MKN 501 (filled square;

Pian et al. 1998). When more than a value of  $\alpha_x$  was available for these BL Lacs we picked the one corresponding to the largest  $\nu_{peak}$ . The  $\nu_{peak}$  values for the sources studied in this paper have been taken from Sambruna, Maraschi & Urry (1996), who fitted a parabola to the  $\nu f_\nu$  broad-band spectra. The  $\nu_{peak}$  values for the HBL studied by Wolter et al. (1998) and Beckmann et al. (2002) are taken from those papers and similarly the values for the additional sources are taken from the referenced papers.

Fig. 5, although with less statistics, basically confirms the *ROSAT* findings, namely a strong anti-correlation between  $\alpha_x$  and  $\nu_{peak}$  for HBL and no correlation for LBL. A few differences, however, are worth mentioning. First, the range in  $\alpha_x$  is somewhat smaller ( $\sim 1.5$  vs.  $\sim 3$ ). This is likely due to the larger energy range over which  $\alpha_x$  is measured (0.1 – 10 keV for *BeppoSAX* vs. 0.1 – 2.4 keV for *ROSAT*). Objects with very steep *ROSAT*  $\alpha_x$ , in fact, are those in which synchrotron emission is nearing the exponential cut-off; by having a larger band *BeppoSAX* includes flatter, higher energy emission due to inverse Compton. Second, the wide 0.1 – 100 keV coverage of *BeppoSAX* has allowed the detection of spectacular spectral variability with  $\nu_{peak}$  reaching  $\gtrsim 10$  keV. As predicted by Padovani & Giommi (1996), these sources display very flat  $\alpha_x$  ( $\sim 0.5$ – $0.8$ ), since *BeppoSAX* is sampling the top of the synchrotron emission. Note that in this case the flat X-ray spectrum is *not* associated with inverse Compton emission, although extreme HBL (objects to the far right in Fig. 5) have X-ray spectra as flat as extreme LBL (objects to the far left of the figure).

## 7 THE 1-JY BL LAC SAMPLE: THE *BeppoSAX* VIEW

*BeppoSAX* data are now available for fourteen 1-Jy BL Lacs: four studied here, seven studied in Paper I, plus MKN 501 (Pian et al. 1998), S5 0716+714 (Giommi et al. 1999), and PKS 0537–441 (Pian et al. 2002). Based on their  $\alpha_{rx}$  and  $\nu_{peak}$  values, 11 objects can be classified as LBL and 3 as HBL, including S5 0716+714 which is an HBL/intermediate source. We note that these sources include *all* 1-Jy BL Lacs with 0.1 – 10 keV X-ray flux larger than  $3 \times 10^{-12}$  erg cm $^{-2}$  s $^{-1}$  (estimated from an extrapolation of the single power-law fits derived for these objects from *ROSAT* data; Urry et al. 1996). This sub-sample is therefore well-defined, makes up a sizeable fraction ( $\sim 41$  per cent) of the full sample, and can therefore be used to obtain robust results on the hard X-ray emission of X-ray bright 1-Jy BL Lacs. Radio data from the UMRAO database are available for ten out of fourteen sources, including MKN 501 and S5 0716+714.

Therefore,  $\sim 71$  per cent of our BL Lacs ( $\sim 73$  per cent of LBL) have nearly simultaneous high-frequency radio data which allow us to study the relationship between X-ray and radio emission almost independently of variability.

### 7.1 The hard X-ray spectra of 1-Jy BL Lacs

The mean value of the LECS/MECS spectral indices, covering the 0.1 – 10 keV range, for the fourteen 1-Jy BL Lacs studied by *BeppoSAX* is  $\langle\alpha_x\rangle = 0.83 \pm 0.07$ . As already indicated by Fig. 5, however, this value reflects two broadly different types of sources and X-ray emission processes.

On one side, in fact, we have the eleven LBL, namely PKS 0048–097, AO 0235+164, PKS 0537–441, OJ 287, PKS 1144–379, OQ 530, PKS 1519–273, S5 1803+784, 3C 371, 4C 56.27, and BL Lac. For these sources the X-ray spectrum is relatively flat, with  $\alpha_x \lesssim 1$  within the errors and  $\langle\alpha_x\rangle = 0.79 \pm 0.07$ . Five of these sources show evidence for a low-energy steepening. While the single  $F$ -test probabilities that the improvement provided by a double power-law model is significant range between 87 and 93 per cent, by adding up the  $\chi^2$  values we derive a 98 per cent probability for the five sources together. The *BeppoSAX* picture for LBL, supported also by their SED, is then that of an inverse Compton dominance, with the steep synchrotron tail coming in around  $\sim 1 - 2$  keV in about half the sources. *ROSAT* data, modulo variability and calibration effects, corroborate the evidence for overall concave spectra. We find, in fact,  $\langle\alpha_x(\text{ROSAT}) - \alpha_x(\text{BeppoSAX})\rangle = 0.55 \pm 0.17$  (and a median value of 0.73). The mean flux ratio (0.1 – 2.4 keV) is  $\langle f_{\text{BeppoSAX}}/f_{\text{ROSAT}}\rangle \sim 0.4$  ( $\sim 0.3$  median), which is again consistent with the picture of a variable synchrotron tail contributing at low energy, thus causing both steeper spectra and higher fluxes when present. This is confirmed also by considering only the five LBL with indication of low-energy steepening: using the broken power-law fit values,  $\langle f_{\text{BeppoSAX}}/f_{\text{ROSAT}}\rangle$  approaches one ( $\sim 0.75$ , with three objects having values  $\sim 1$  and two  $\sim 0.4 - 0.5$ ).

On the other side, we have the three HBL, namely S5 0716+714, MKN 501, and PKS 2005–489. The mean value in this case is  $\langle\alpha_x\rangle = 1.0 \pm 0.2$ , which increases to  $\langle\alpha_x\rangle = 1.2 \pm 0.1$  if we exclude MKN 501, found in an extremely high state, with very large  $\nu_{\text{peak}}$  and a flat synchrotron spectrum, as predicted by the correlation shown in Fig. 5. The evidence for spectral curvature here is mixed. While MKN 501 shows flattening at lower energies ( $\Delta\alpha_x \sim -0.2$  below  $\sim 2$  keV; Pian et al. 1998), S5 0716+714 shows steepening ( $\Delta\alpha_x \sim 0.7$  below  $\sim 2 - 3$  keV; Giommi et al. 1999). This difference can be explained by looking at Fig. 5. While S5 0716+714 is an HBL with  $\nu_{\text{peak}} \sim 10^{15}$  Hz, and therefore relatively close to LBL values, MKN 501 was observed by *BeppoSAX* in outburst, with  $\nu_{\text{peak}} \gtrsim 100$  keV or  $\gtrsim 2 \times 10^{19}$  Hz. In one case we are then seeing a mix of synchrotron and inverse Compton radiation, while in the other we are looking at the overall steepening of pure synchrotron emission. The *BeppoSAX* picture for HBL, supported also by their SED, is then that of a synchrotron dominance, with the flat inverse Compton component making a contribution for intermediate sources. As regards *ROSAT* data, we get  $\langle\alpha_x(\text{ROSAT}) - \alpha_x(\text{BeppoSAX})\rangle = 0.89 \pm 0.03$  (and a median value of 0.92). The mean flux ratio is  $\langle f_{\text{BeppoSAX}}/f_{\text{ROSAT}}\rangle \sim 1.5$  ( $\sim 1.5$  median), a factor  $\sim 4$  larger than for the LBL. The mean

flux ratio at 1 keV is a factor  $\sim 7$  larger for HBL than for LBL.

We note that large variability has been seen in the synchrotron component of several BL Lacs observed with *BeppoSAX* (Ravasio et al. 2002, and references therein) and possibly only once, to the best of our knowledge, in their inverse Compton component (in the case of PKS 1144–379: Paper I). Comparing single power-law fits, however, one should be aware of another factor that could contribute to different values of  $f_{\text{BeppoSAX}}/f_{\text{ROSAT}}$  for HBL and LBL. As pointed out by Beckmann et al. (2002), the different X-ray spectral shapes of HBL and LBL could play a role, given the different spectral response of the two instrument. LBL have flat inverse Compton spectra but synchrotron emission, with a steep spectrum, sometimes dominates at soft energies (in  $\sim 45$  per cent of our sources). The fits to their *BeppoSAX* LECS/MECS spectra, which sample a much larger range towards high energies than the *ROSAT* PSPC spectra, may then be mostly sensitive to the flat inverse Compton component, with the result that the fitted flux at 1 keV (and integrated in the soft band) is lower than that inferred from the *ROSAT* fits. This effect is less important when a broken power-law is adopted (see above), but the relatively low statistics of the LECS data may not always justify a statistical preference of this model with respect to the single power-law one.

### 7.2 X-ray and radio powers and $\alpha_{\text{rx}}$

As mentioned above, since  $\sim 70$  per cent of the objects have nearly simultaneous X-ray and radio data, we can address the relation between X-ray and radio emission almost independently of variability. Fig. 6 plots the radio power  $L_r$  vs. the X-ray power  $L_x$  for our sources. As expected, the HBL, having larger  $\nu_{\text{peak}}$  values, have larger  $L_x$  at a given  $L_r$  and therefore occupy the bottom-right part of the diagram. The correlation between  $L_r$  and  $L_x$  for LBL is surprisingly tight, strong, and linear. We find  $L_r \propto L_x^{0.99 \pm 0.08}$ , significant at the  $> 99.99$  per cent level. A partial correlation analysis (e.g., Padovani 1992), shows that the correlation is still very strong ( $P \sim 99.7$  per cent) even when the common redshift dependence of the two powers is subtracted off. Equivalently,  $\alpha_{\text{rx}}$  has a very small dispersion for LBL. We get  $\langle\alpha_{\text{rx}}\rangle = 0.861 \pm 0.008$  (dashed line in Fig. 6). Given the tightness of the correlation, and the importance that the suggested strong link between the radio and X-ray band would have for LBL, we have looked in the UMRAO database for radio observations at 4.8 GHz nearly simultaneous with the *ROSAT* data presented by Urry et al. (1996). This provided us with 11 more sources, for a total of 22 1-Jy LBL,  $\sim 86$  per cent of them with nearly simultaneous X-ray and radio data. The results obtained for our *BeppoSAX* sources are confirmed with this enlarged sample. Namely, we find now  $L_r \propto L_x^{0.97 \pm 0.08}$ , significant at the  $> 99.99$  per cent level. As before, the correlation is still very strong ( $P \sim 99.97$  per cent) when the common redshift dependence is subtracted off. We get  $\langle\alpha_{\text{rx}}\rangle = 0.89 \pm 0.01$  (dotted line in Fig. 6) for the 11 *ROSAT* sources, not significantly different from our previous value, and a mean for the 22 1-Jy LBL of  $\langle\alpha_{\text{rx}}\rangle = 0.875 \pm 0.008$ . This means that the X-ray power (or flux) can be extrapolated from the radio power (or flux)

within  $\sim 15$  per cent over almost eight orders of magnitude in frequency.

It is interesting to note that the strong  $L_r - L_x$  correlation displayed by the 1-Jy LBL is *not* only due to the nearly simultaneous radio and X-ray data. Even if we use the original 1-Jy data, in fact, we find a strong correlation ( $P > 99.99$  per cent) for the 22 sources in Fig. 6, still very significant ( $P \sim 99.97$  per cent) when the redshift effect is subtracted off. The slope of the correlation is slightly flatter and  $\langle \alpha_{rx} \rangle$  is slightly larger (although not significantly so:  $0.890 \pm 0.008$ ), as on average the 1 Jy fluxes are larger than the UMRAO ones, but the dispersion is still very small. We note that the relatively small range in  $\langle \alpha_{rx} \rangle$  for LBL, although never studied with nearly simultaneous radio and X-ray data, has been previously noted, amongst others, by Padovani & Giommi (1995) and Fossati et al. (1998). To the best of our knowledge, however, all previous studies of the  $L_r - L_x$  correlation for 1-Jy BL Lacs did not distinguish between LBL and HBL, thereby reducing the significance of the correlation.

The interpretation of the strong linear link between X-ray and radio emission components in LBL suggested by the  $L_r - L_x$  correlation is not straightforward within the currently accepted scenario. As illustrated in Fig. 4, in fact, our one-zone model cannot reproduce the observed radio flux, thought to originate in a region of the jet larger than the (more compact) one responsible for most of the emission, including X-rays. On the other hand, since the radio spectra in these sources are invariably flat, there is a correlation between the radio flux at the self-absorption frequency ( $\sim 10^2 - 10^3$  GHz) of the smaller X-ray emitting region and the flux at 5 GHz. This may account, at least in part, for the  $L_r - L_x$  correlation, even if the powers in the two bands are produced in different parts of the jet.

## 8 CONCLUSIONS

We have presented new *BeppoSAX* observations of four BL Lacertae objects selected from the 1-Jy sample, all LBL, i.e., characterized by a peak in their multifrequency spectra at infrared/optical energies. We have then used these data plus data previously published by us (7 sources; Paper I) and others (3 sources) to study the properties of the hard X-ray spectra of an X-ray flux-limited 1-Jy sub-sample (containing 11 LBL and 3 HBL) and constrain the emission processes.

A relatively simple picture comes out from this paper: a dominance of inverse Compton emission in the X-ray band of LBL, with  $\sim 50$  per cent of the sources showing also a likely synchrotron component. Our main results are as follows:

(i) The *BeppoSAX* spectra of our LBL sources are relatively flat ( $\alpha_x \sim 0.8$ ). For five sources broken power-law models improve the fits at the 98 per cent level when the  $\chi^2$  values for the single sources are added up. The resulting best-fit spectra all concur in indicating a flatter component emerging at higher energies, with spectral changes  $\Delta\alpha_x \sim 0.8$  around 1 – 2 keV.

(ii) Our LBL have a typical difference between *BeppoSAX* and *ROSAT* spectral slopes  $\alpha_x(\text{ROSAT}) - \alpha_x(\text{BeppoSAX}) \sim 0.6$ . The interpretation of this effect is complicated by possible *ROSAT* miscalibrations (which, if at all present, could explain a difference  $\sim 0.3$ ) and variability effects, as the

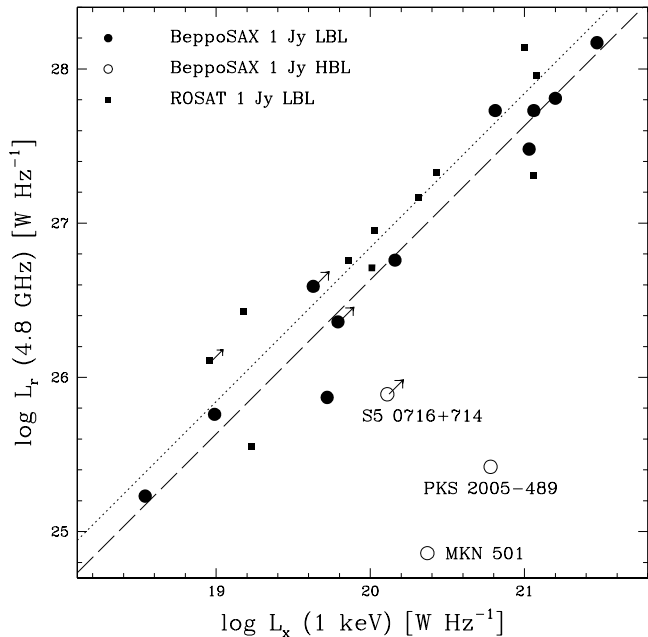


**Figure 6.** Nearly simultaneous X-ray and radio luminosities of 1-Jy BL Lacs objects observed by *BeppoSAX* (circles) and *ROSAT* (squares). Lower limits indicate sources for which no redshift is available but  $z > 0.2$  was assumed, based on the fact that the host galaxies are optically unresolved. The dashed line indicates a value of  $\alpha_{rx} = 0.861$ , the mean value for the *BeppoSAX* LBL, while the dotted line indicates a value of  $\alpha_{rx} = 0.89$ , the mean value for the *ROSAT* LBL. Labels identify the HBL (open circles).

mean flux ratio is  $\langle f_{\text{BeppoSAX}}/f_{\text{ROSAT}} \rangle \sim 0.4$ , but is consistent with the picture of a variable synchrotron emission contributing in the soft X-ray band, leading to high fluxes and steeper spectra when present.

(iii) Despite the non-simultaneity of the multifrequency data (UMRAO radio data excluded) it is apparent that the *BeppoSAX* spectra indicate a different emission component in the SEDs of our LBL sources, separate from that responsible for the low energy emission. In fact, the extrapolation of the relatively flat *BeppoSAX* slopes cannot be extended to much lower frequencies since the predicted optical flux would be orders of magnitude below the observed value. A sharp steepening towards lower frequencies is then necessary to meet the much higher optical (synchrotron) flux.

(iv) Our interpretation of the  $\alpha_x - \nu_{\text{peak}}$  diagram is the one originally proposed by Padovani & Giommi (1996) for the *ROSAT* data. Namely,  $\alpha_x$  steepens moving from LBL to HBL as synchrotron replaces inverse Compton as the main emission mechanism in the X-ray band. The spectral index then flattens again as the synchrotron peak moves to higher energies in the X-ray band, eventually converging to the relatively flat value characteristic of synchrotron emission before the peak. Again, this fits perfectly with a dominance of inverse Compton emission in our LBL.

(v) We find a very tight proportionality between nearly simultaneous radio and X-ray powers for our LBL sources and 11 additional LBL with *ROSAT* data, such that X-ray power can be predicted within  $\sim 15$  per cent from the radio

power. This points to a strong link between X-ray and radio emission components in LBL.

(vi) The data for the (small number of) HBL are consistent with other studies based on larger samples of sources and confirm the dominance of synchrotron emission in the *BeppoSAX* band.

## ACKNOWLEDGEMENTS

We thank Andrea Comastri, Giovanni Fossati, Franco Mantovani, Laura Maraschi, Carlo Stanghellini, Gianpiero Tagliaferri, and Meg Urry for their contribution at an early stage of this project. LC acknowledges the STScI Visitor Program. This research has made use of data from the University of Michigan Radio Astronomy Observatory which is supported by funds from the University of Michigan and of the NASA/IPAC Extragalactic Database (NED), which is operated by the Jet Propulsion Laboratory, California Institute of Technology, under contract with the National Aeronautics and Space Administration.

## REFERENCES

Beckmann V., Wolter A., Celotti A., Costamante L., Ghisellini G., Maccacaro T., Tagliaferri G., 2002, *A&A*, 383, 410  
 Boella G. et al., 1997a, *A&AS*, 122, 299  
 Boella G. et al., 1997b, *A&AS*, 122, 327  
 Burbidge E. M., Beaver E. A., Cohen R. D., Junkkarinen V. T., Lyons R. W., 1996, *AJ*, 112, 2533  
 Celotti A., Padovani P., Ghisellini G., 1997, *MNRAS*, 286, 415  
 Dickey J. M., Lockman F. J., 1990, *ARAA*, 28, 215  
 Donato D., Ghisellini G., Tagliaferri G., Fossati G., 2001, *A&A*, 375, 739  
 Elvis M., Lockman F. J., Wilkes, B. J., 1989, *AJ*, 97, 777  
 Fiore F. et al., 1999, *Handbook for NFI Spectral Analysis*, available at <http://www.asdc.asi.it/bepposax/software/>  
 Fossati G., Maraschi L., Celotti A., Comastri A., Ghisellini G., 1998, *MNRAS*, 299, 433  
 Fossati G. et al., 2000, *ApJ*, 541, 166  
 Frontera F. et al., 1997, *A&AS*, 122, 357  
 Gehrels N., 1986, *ApJ*, 303, 336  
 Ghisellini G., Celotti A., Fossati G., Maraschi L., Comastri A., 1998, *MNRAS*, 301, 451  
 Ghisellini G., Celotti A., Costamante L., 2002, *A&A*, 386, 833  
 Giommi P., Fiore, F., 1997, 5th Int. Workshop on Data Analysis in Astronomy, Erice. World Scientific Press, Singapore, p. 93  
 Giommi P., Padovani P., 1994, *MNRAS*, 268, L51  
 Giommi P., Padovani P., Perlman E., 2000, *MNRAS*, 317, 743  
 Giommi P. et al., 1998, *A&A*, 333, L5  
 Giommi P. et al., 1999, *A&A*, 351, 59  
 Heidt J., Wagner S. J., 1996, *A&A*, 305, 42  
 Iwasawa K., Fabian A. C., Nandra K., 1999, *MNRAS*, 307, 611  
 Kaspi S., Smith P. S., Netzer H., Maoz D., Jannuzi B. T., Giveon U., 2000, *ApJ*, 533, 631  
 Kollgaard R. I., 1994, *Vistas Astron.*, 38, 29  
 Lamer G., Brunner H., Staubert R., 1996, *A&A*, 311, 384  
 Lin Y. C. et al., 1999, *ApJ*, 525, 191  
 Madejski G., Takahashi T., Tashiro M., Kubo H., Hartman R., Kallman T., Sikora, M., 1996, *ApJ*, 459, 156  
 Mineo T. et al., 2000, *A&A*, 359, 471  
 Morrison R., McCammon D., 1983, *ApJ*, 270, 119  
 Murphy E. M., Lockman F. J., Laor A., Elvis M., 1996, *ApJS*, 105, 369  
 Padovani P., 1992, *A&A*, 256, 399

Padovani P., Giommi P., 1995, *ApJ*, 444, 567  
 Padovani P., Giommi P., 1996, *MNRAS*, 279, 526  
 Padovani P. et al., 2001, *MNRAS*, 328, 931 (Paper I)  
 Padovani P., Costamante L., Ghisellini G., Giommi P., Perlman E., 2002, *ApJ*, 581, 895  
 Parmar A. et al., 1997, *A&AS*, 122, 309.  
 Pian E. et al., 1998, *ApJ*, 492, L17  
 Pian E. et al., 2002, *A&A*, 392, 407  
 Puchnarewicz E. M. et al., 1997, *MNRAS*, 291, 177  
 Ravasio M. et al., 2002, *A&A*, 383, 763  
 Sambruna R., Maraschi L., Urry C. M., 1996, *ApJ*, 463, 444  
 Spada M., Ghisellini G., Lazzati D., Celotti A., 2001, *MNRAS*, 325, 1559  
 Stickel M., Padovani P., Urry C. M., Fried J. W., Kühr H., 1991, *ApJ*, 374, 431  
 Tagliaferri G. et al., 2000, *A&A*, 354, 431  
 Tagliaferri G. et al., 2003, *A&A*, 400, 477  
 Urry C. M., Padovani, P., 1995, *PASP*, 107, 803  
 Urry C. M., Sambruna R. M., Worrall D. M., Kollgaard R. I., Feigelson E. D., Perlman E. S., Stocke J. T., 1996, *ApJ*, 463, 424  
 Wolter A. et al., 1998, *A&A*, 335, 899